Molecular Origin of the Charge Carrier Mobility in Small Molecule Organic Semiconductors

*Pascal Friederich, Velimir Meded, Angela Poschlad, Tobias Neumann, Vadim Rodin, Vera Stehr, Franz Symalla, Denis Danilov, Gesa Lüdemann, Reinhold F. Fink, Ivan Kondov, Florian von Wrochem, and Wolfgang Wenzel**

Small-molecule organic semiconductors are used in a wide spectrum of applications, ranging from organic light emitting diodes to organic photovoltaics. However, the low carrier mobility severely limits their potential, e.g., for large area devices. A number of factors determine mobility, such as molecular packing, electronic structure, dipole moment, and polarizability. Presently, quantitative ab initio models to assess the influence of these molecule-dependent properties are lacking. Here, a multiscale model is presented, which provides an accurate prediction of experimental data over ten orders of magnitude in mobility, and allows for the decomposition of the carrier mobility into molecule-specific quantities. Molecule-specific quantitative measures are provided how two single molecule properties, the dependence of the orbital energy on conformation, and the dipole-induced polarization determine mobility for hole-transport materials. The availability of first-principles based models to compute key performance characteristics of organic semiconductors may enable in silico screening of numerous chemical compounds for the development of highly efficient optoelectronic devices.

P. Friederich, Dr. V. Meded, Dr. T. Neumann,
F. Symalla, Dr. D. Danilov, Prof. W. Wenzel
Institute of Nanotechnology (INT)
Karlsruhe Institute of Technology
Hermann-von-Helmholtz-Platz 1
76344 Eggenstein-Leopoldshafen, Germany
E-mail: wolfgang.wenzel@kit.edu

Dr. A. Poschlad, Dr. I. Kondov
Steinbuch Centre for Computing (SCC)
Karlsruhe Institute of Technology
Hermann-von-Helmholtz-Platz 1
76344 Eggenstein-Leopoldshafen, Germany

Dr. V. Rodin, Dr. G. Lüdemann,[+] Dr. F. von Wrochem
Materials Sciences Laboratory
Sony Deutschland GmbH
Hedelfinger Str. 61, 70327 Stuttgart, Germany

Dr. V. Stehr
Institute of Physical and Theoretical Chemistry
University of Würzburg
Am Hubland – Campus Süd, 97074 Würzburg, Germany

Prof. R. F. Fink
Institute for Physical and Theoretical Chemistry
University of Tübingen
Auf der Morgenstelle 18, 72076 Tübingen, Germany

1. Introduction

The discovery of electroluminescence in organic semiconductors has sparked intense research efforts to exploit these materials in applications for energy conversion, which culminated in the development of organic light emitting diodes[1] for displays and lightning and has shown promise for applications in photovoltaics.[2] One of the most severe limiting factors of organic semiconductors is the low carrier mobility [$\mu \cong 10^{-10}$–10^{1} cm^2 (V^{-1}s^{-1})[3]], which falls short of the mobility in inorganic materials by five to ten orders of magnitude [$\mu \cong 10^{2}$–10^{4} cm^2 (V^{-1}s^{-1})]. One of the reasons for this discrepancy is the relevance of hopping transport in disordered organic semiconductors. In particular in many small molecule organic semiconductors, electron or hole polarons traverse the material by a hopping process, which can be locally described by Marcus theory.[4] The rate to hop between two sites in the materials is given by

$$k_{if} = \frac{2\pi}{\hbar}|J_{if}|^2 \frac{1}{\sqrt{4\pi\lambda_{if}k_B T}} \exp\left(-\frac{(\lambda_{if}+\Delta G_{if})^2}{4\lambda_{if}k_B T}\right) \quad (1)$$

where k_B is the Boltzmann constant and T is the temperature. J_{if}[5] are hopping (or electronic coupling) matrix elements, λ_{if} is the reorganization energies and ΔG_{if} is the change in Gibbs free energy accompanied with a charge carrier hopping from the initial (i) and final (f) molecule. The small polaron model assumed in Equation (1) is applicable when the intermolecular coupling is smaller than the reorganization energy,[6] a condition fulfilled for all materials considered in this work. Equation (1) leads to an exceptionally strong dependence of the mobility on the width of the disorder distribution σ of the polaron site energies in the material, i.e., $\mu \propto \exp\left[-C\left(\frac{\sigma}{k_B T}\right)^2\right]$, where C is a constant chosen to either fit the experiment or an appropriate theory[7] (see Supporting Information). The molecular origin of many factors[8] influencing the polaron mobility either directly (e.g., dipole moment) or indirectly (e.g., molecular packing[9]) has been studied intensively over many decades and many fundamental aspects of polaron transport in organic semiconductors

are now well understood, in part by the seminal work of Bässler and co-workers.[7g,10] However, despite these efforts predictive models to quantify these influences on the charge carrier mobility a priori are presently lacking.[8a,c] Such an approach requires many ingredients, such as an accurate description of the morphology and the electronic structure in the matrix. We present a first-principles-based multi-scale approach[11] (**Figure1**) to compute the hole mobility of nine widely used small molecule organic semiconductors, i.e., Alq_3, α-NPD, DEPB, mBPD, NNP, pFFA, TPD, TET, and PEN (abbreviations are explained in Experimental Section). The compounds represent a wide range of experimentally used organic semiconductors, e.g., Alq_3 is used as electron transport layer (ETL), whereas α-NPD is an established hole transport layer (HTL) material. The first seven materials form disordered films, while the last two are crystalline. We note that the mobility of these materials vary over ten orders in magnitude, which represents a challenge for any modelling approach.

2. Simulation Methods

The mobility was computed in a complex multiscale simulation approach, which is illustrated in Figure 1. We first generate atomistically resolved morphologies of the materials in an amorphous solid phase. To this end, we perform molecular dynamics simulations. We generate amorphous morphologies including 300 molecules each with periodic boundary conditions (details in Experimental Section below). For all systems, the final morphologies have a disordered structure without any indications of crystalline domains. Crystalline structures of pentacene and tetracene are obtained from Schiefer et al.[12] Next, the electronic structure of the molecules in the matrix must be characterized.[8a,11a,13] Here, we use the fully ab initio Quantum Patch method[11a] on periodically extended structures incorporating 8100 molecules as embedding. We compute pairwise electron coupling matrix elements (J_{if}) for ≈600 pairs, reorganization energies (λ_{if}), and site energy differences (ΔE_{if}) including the environmental effects (polarization and conformational disorder). In the Quantum Patch approach,[11a] the Schrödinger equation for systems of weakly coupled molecules is solved numerically in a self-consistent manner. The electrostatic interaction between molecules, which crucially influences the molecule specific site energy, is modeled by atom-centered partial charges that are self-consistently determined. This approach thus permits an ab initio characterization of the polarization effects, which are critical to describe the electronic disorder in the system. We calculate the inner part of the reorganization energy λ based on the Nelsen's four point procedure.[14] Traditionally the reorganization energy has been calculated in vacuum, where a full relaxation of the molecule is possible. Such complete conformational freedom is unrealistic when the molecules are confined in the matrix. For the molecules investigated here, the internal degrees of freedom which are most affected by confinement in the matrix are the dihedral angles, which are fixed during the formation of the solid phase. We have therefore implemented a novel procedure, the frozen-dihedral approach, where we compute the reorganization energy in the solid phase by constraining the dihedral angles for each molecule at the values obtained in the morphology and only permit relaxation of the other degrees of freedom (such as breathing and angle-relaxations), which do not result in large-scale conformation changes.[15] The hopping matrix elements J for each molecule in the converged electrostatic environment to all of its neighbors are calculated by using the Löwdin orthogonalization[5,16] procedure for the highest occupied molecular orbitals (HOMO). To this end, we extract both frontier orbitals and Fock- and overlap matrices are extracted from monomer/dimer calculations in a sufficiently large embedding environment (see Results) calculated in the Quantum Patch method, consisting of at least several hundreds of molecules per system. Thus, we obtain a distance dependent distribution of hopping matrix elements for each system. For completeness, a similar procedure was applied for lowest unoccupied molecular orbitals (LUMO), as well.

Statistical averages of these microscopic materials characteristics are used as input in the generalized effective medium model (GEMM).[17] In the GEMM the mobility is obtained from an analytic solution of the master equation within the effective medium approximation:

$$\mu = \frac{e\beta M < J^2 r^2 >}{n\hbar\sqrt{\lambda}} \sqrt{\frac{\pi\beta}{1+\frac{\beta\sigma^2}{\lambda}}} \exp\left[-C\left((\beta\sigma)^2 - \beta\lambda\right)\right] \quad (2)$$

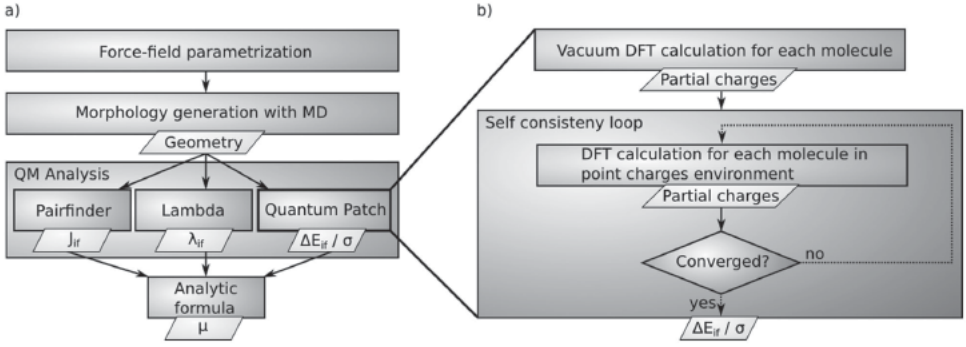

Figure 1. A flowchart representation of the workflow: In a) the general workflow is shown. We start with morphology generation followed by quantum mechanical (QM) microscopic analysis and finish by feeding the parameters obtained in QM step into the mobility expression. In b) details of the Quantum Patch method are being displayed. A self-consistency procedure is used where the single molecules are embedded in partial charges of the environment until the partial charges of each molecule are converged with molecular total energies as convergence criterion.

Here, e is the electron charge, $\beta = 1/k_B T$ is the inverse temperature, $n = 3$ is the dimension of the charge transport, and M is the mean number of the nearest-neighbor molecules, $\hbar$ is the reduced Planck constant, and $\langle J^2 r^2 \rangle$ and λ are averages over the hopping matrix elements[11a] and pairwise reorganization energies, respectively. As in prior work, we use the GEMM model with $C = 1/4$, corresponding to the effective medium limit, which best agrees with the experimental data (Figure S3, Supporting Information). Complex models[7d] with C-factors, which depend on the interplay between energy disorder and the reorganization energy have been discussed in the literature. As pointed out by Bässler and co-workers,[10] this relationship depends on molecular connectivity and off-diagonal disorder. These models are compared to kinetic Monte Carlo (KMC) calculations performed on perfect rectangular lattices. Rodin et al.[17] pointed out that connectivity may actually be different for real morphologies when compared to perfect lattices. Therefore, we use the approach (Equation (2)) with $C = 0.25$.

3. Results and Discussion

Figure2 a shows the comparison of the computed charge carrier mobility with experimental data for the materials in question (the corresponding microscopic parameters are summarized in **Table1**). As anticipated, the polaron energies are well described by Gaussian distributions,[7g,10] while the hopping matrix elements follow an exponential envelope. The distribution of the on-site energy differences, which crucially influence the Marcus hopping rates, is shown in Figure 2b for two specific materials, NNP and pFFA. To illustrate the point we note that NNP has a 21% larger disorder width than pFFA and consequently an order of magnitude lower mobility, even though the remaining microscopic parameters are quite comparable. Figure 2c shows the electronic coupling matrix elements for two molecules, namely Alq_3 and pFFA, for comparison. Alq_3 is a compact "sphere-like" molecule with a narrow distribution of hopping matrix elements, which decays exponentially with distance. pFFA, a more extended and flexible molecule, displays a rather diffuse and wide-spread distribution of coupling matrix elements. This leads to an overall reduction of $\langle J^2 r^2 \rangle$ by an order of magnitude (9.99×10^{-3} eV²Å² for Alq_3 vs. 1.46×10^{-3} eV²Å² for pFFA, see Table 1**)**. As $\langle J^2 r^2 \rangle$ in the prefactor in Equation (2) only linearly influences the charge carrier mobility, the key parameter affecting the mobility trend is still the larger disorder width σ of Alq_3.

We note that the observed agreement with experimental data can only be achieved if the reorganization energies are evaluated in the frozen dihedral approximation (see Supporting Information). The reorganization energy, i.e., the energy difference between the relaxed and unrelaxed structure of a molecule when charge hops from donor to acceptor was computed using Nelsen's four-point procedure.[14] In solution, the relaxation of the molecule is typically unconstrained. In a solid-state matrix,

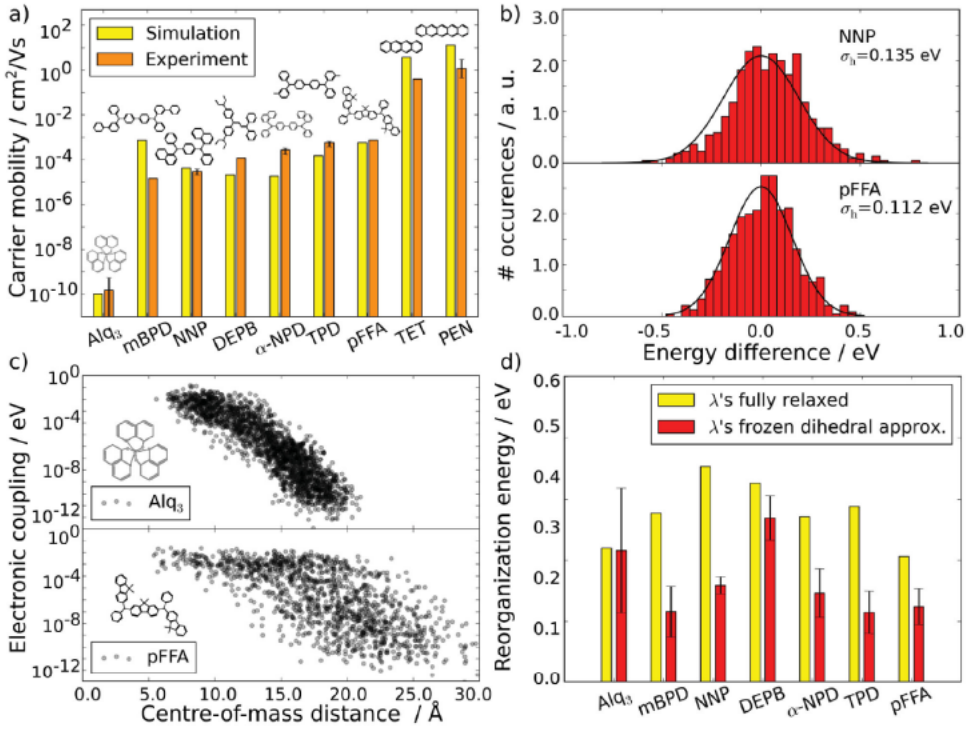

Figure 2. a) Comparison of hole mobilities of nine different organic semiconductors varying from poorly conducting Alq_3 to highly conducting crystalline materials, such as tetracene and pentacene. Predictions from the first-prinicples workflow are in agreement with experiment within one order of magnitude for all materials. b) Distribution of energy differences computed with the quantum patch method for NNP and pFFA. The width of the distribution yields the energy disorder, the main determinant of the mobility. c) Distance dependence of electronic couplings for a compact (Alq_3) and a more extended molecule (pFFA). d) Reorganization energies in the fully-relaxed (yellow) and frozen-dihedral approximation (red) differ significantly for mBPD, NNP, α-NPD, TPD, and pFFA.

Table 1. Microscopic input parameters and hole mobilities of the analyzed molecules (see Figure S1, Supporting Information). The charge mobility depends on the disorder strength (σ), the frozen dihedral reorganization energy λ and a prefactor $\langle J^2 r^2 \rangle$ incorporating the hopping matrix elements (see text and Supporting Information for definitions). The last column gives literature values of the experimental mobility.

	σ [eV]	σ_i [eV]	σ_p [eV]	ΔE_{int}^{HOMO} [eV]	$\langle J^2 r^2 \rangle$ [eV^{2}Å^2]	M	λ [eV]	μ sim. [cm^2 V^{-1}s^{-1}]	μ exp. [cm^2 V^{-1}s^{-1}]
Alq_3	0.224	0.166	0.151	–	9.99×10^{-3}	7.31	0.296	1.01×10^{-10}	1.46×10^{-10}[33]
mBPD	0.110	0.080	0.075	0.186	1.52×10^{-3}	8.52	0.143	7.38×10^{-4}	1.49×10^{-5}[34]
NNP	0.135	0.137	–	0.431	1.64×10^{-3}	7.65	0.160	4.31×10^{-5}	2.99×10^{-5}[35]
DEPB	0.130	0.086	0.098	0.272	1.42×10^{-3}	8.16	0.266	2.09×10^{-5}	1.17×10^{-4}[36]
α-NPD	0.144	0.126	0.070	0.250	2.04×10^{-3}	7.73	0.158	1.84×10^{-5}	2.70×10^{-4}[33b,37]
TPD	0.129	0.097	0.084	0.197	1.56×10^{-3}	8.49	0.110	1.52×10^{-4}	5.74×10^{-4}[33b,d,36,38]
pFFA	0.112	0.100	0.049	0.366	1.46×10^{-3}	7.70	0.134	5.70×10^{-4}	7.60×10^{-4}[34]
TET	0.0	0.0	0.0	–	1.13×10^{-2}	15.8	0.114	3.83	0.4[39]
PEN	0.0	0.0	0.0	–	3.07×10^{-2}	15.8	0.097	13.35	3.0/21[20,21]

large-scale conformational changes are strongly hindered by the matrix surrounding. For the molecules under study, this refers mostly to dihedral angle changes. We have therefore computed both the full reorganization energy (all degrees of freedom are free to relax), and the reorganization energy with constrained dihedral angles. The latter approach, termed frozen dihedral approximation, reduces the average reorganization energy (see Figure 2d and S1b, Supporting Information as well as Experimental Section) for all materials, but also leads to molecule-specific differences by as much as 50%, which in turn affects the mobility estimate. The true reorganization energy of a molecule in the matrix is expected to lie between the frozen-dihedral and the free reorganization energies.

To analyze the molecular parameters that determine the mobility, Equation (2) is decomposed as

$$\log \mu = \log \mu_0 - C\beta\lambda - C\beta^2\left(\sigma_i^2 + \sigma_p^2\right) \tag{3}$$

where μ_0 is the prefactor of the exponential, β and C are defined as in Equation (2). We decomposed the energy disorder width σ into an intrinsic and a polarization component. The intrinsic contribution σ_i arises from the molecular packing, i.e., conformational disorder, whereas the polarization part σ_p arises from the electrostatic surrounding of the molecule induced by the matrix. As the physical nature of these contributions to the total energy is fundamentally different, we treat them as uncorrelated as a first approximation in this study, which means that the square of the width of the full disorder distribution is the sum of the individual contributions. The intrinsic component of the disorder σ_i is extracted from the Quantum Patch calculations by calculating single molecule energy level variance on molecules extracted from the matrix, i.e., taking only the structural (conformational) part of the environmental effect[11a] (see Supporting Information for details). Conversely, the polarization contribution $\sigma_p^2 = \sigma^2 - \sigma_i^2$, represents the electronic (polarization) effect of the environment.

In **Figure 3**, we show the decomposition of the molecular contributions to the mobility. The mobility μ_0 (the blue bars) can be interpreted as the mobility of a fictional material comprised of fully constrained molecules (without energy disorder or reorganization energy). Interestingly, μ_0 is of the same order of magnitude for all disordered materials under study. The μ_0 values of these materials, which are still significantly lower than those of high-purity band-transport crystalline semiconductors, provide an order-of-magnitude estimate of the maximal mobility attainable by amorphous small-molecule organic semiconductors. However, due to differences in dominant molecular properties, in particular dipole moments and intrinsic disorder, the actual mobility is orders of magnitude lower.

A first reduction of μ_0 arises from the reorganization effects according to Marcus theory. However, the variation of the mobility (green bars) is smaller than one order of magnitude, and again quite similar for all materials under study. This data can be interpreted as the mobility in a fictional crystalline material of the same molecular composition as the amorphous material. Finally, as extensively discussed in literature,[18] the electrostatic polarization (yellow bars) plays a major role in determining the mobility of the material. In agreement with arguments made by Bässler and co-workers,[18,19] we observe a strong correlation between the dipole moment of a molecule and its disorder/charge mobility, as illustrated in **Figure 4**a. Even though the hopping approach may not be fully appropriate to describe the mobility in crystalline materials it is interesting to consider these materials as points-of-reference in his approach: The crystallinity and rigidity of pentacene and tetracene lead to vanishingly small disorder. Consequently, for these materials the charge mobility is dominated by the coupling matrix elements and the reorganization energy. In Figure 2a, we show the hole mobility of pentacene obtained from thin-film transistors (3 cm^2 V^{-1}s^{-1})[20] as well as from THz experiments (21 cm^2 V^{-1}s^{-1}).[21] The predicted charge mobility simulated for an idealized, single crystalline system (13 cm^2 V^{-1}s^{-1} for pentacene) overestimates the thin-film transistor mobility while it is closer to the value observed in THz experiments,[21] where grain boundaries do not play a role. However, we note that without analysis of the temperature dependence of the charge carrier mobility, it is unclear whether the model of activated hopping transport is fully applicable, or whether delocalized states or even band transport are relevant for transport in these materials.

The molecules mBPD–pFFA (in the indicated frame in Figure 4b) have intrinsically small dipole moments

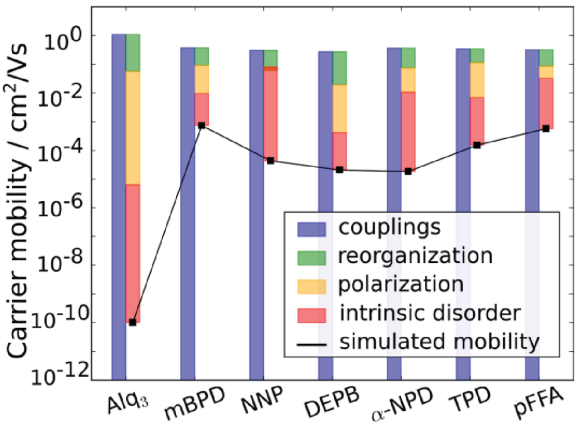

Figure 3. Breakdown of the charge mobility (log scale) in four parts: A disorder and reorganization-energy independent part (blue), the effect of reorganization (green) and disorder. The disorder is again subdivided into environmental effects (yellow) and intrinsic effects (red). For most disordered HTL materials the largest contribution of to the variation of the mobility arises from the intrinsic disorder.

(1.5–4 Debye), and therefore only weak electrostatic interactions. As a result, polarization plays only a moderate role for these systems. However, Alq_3 exhibits a large intrinsic dipole moment (>6 Debye), and the high polarization induced by the dipoles leads to the lowest mobility among the materials studied, indicating that the intrinsic molecular dipole has to be optimized with great care when designing new materials.

A second crucial contribution to the true mobility is the intrinsic (conformational) disorder, which arises from the fact that molecules are distorted when packed into the matrix (see Figure 3). Surprisingly, this contribution dominates the variation of the carrier mobility for all noncrystalline materials with small dipole moment, e.g., typical HTL, as illustrated in Figure 4a. To analyze the origin of this variation, we consider the geometry of molecules in the matrix of the disordered film: the molecular position and conformation in the bulk result from a trade-off between maximizing intermolecular interactions, while minimizing energy penalties arising from the distortion of the molecule that is required to fit into the disordered material. As already alluded to in the discussion of the reorganization energy, the lowest-energy degrees of freedom of these molecules are rotations around the dihedral angles, which results in significant change of the molecular shape at little energy cost. However, these distortions also lead to a shift in the polaron energy on this site, to the lowest order approximated by the change of the HOMO energy (see Figure 4b–d) as a function of a single, arbitrarily chosen dihedral angle. HOMO distributions resulting from rotations around different dihedral angles show analogue behavior (see Supporting Information).

To develop a quantitative and molecule specific model for the origin of the intrinsic disorder contribution in organic materials, in the top panels of Figure 4c,d the distribution of

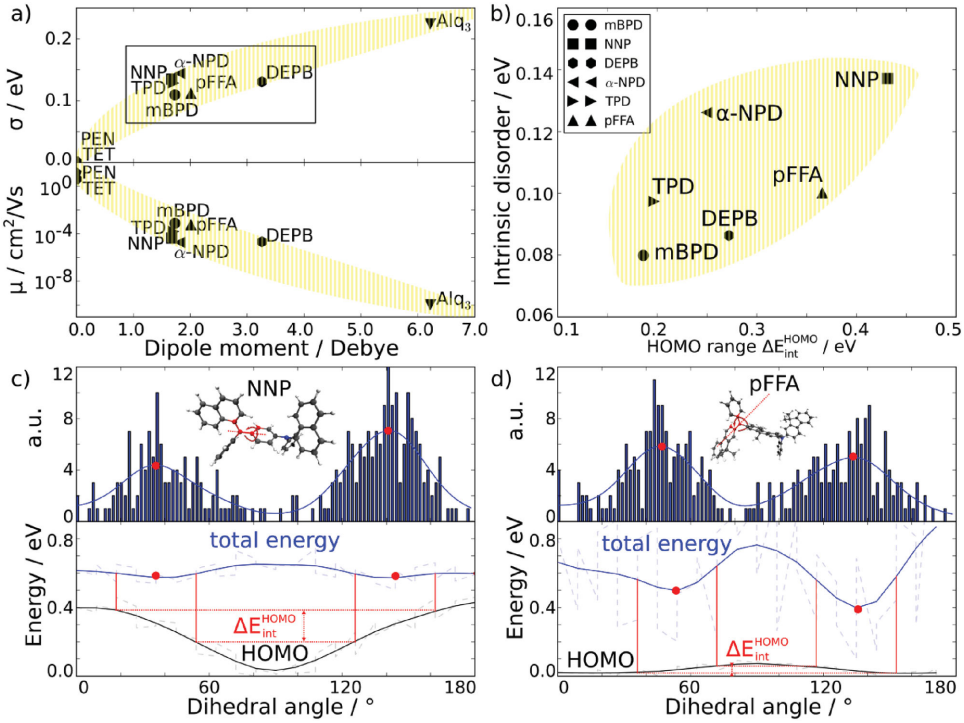

Figure 4. a) Correlation between energy disorder (upper panel)/mobility(lower panel) and the dipole moments of the molecule in the matrix. The HTL molecules in the frame are analyzed in b). b) Correlation between the intrinsic energy disorder (σ_i) and the HOMO energy variance (ΔE_{int}^{HOMO}). The variation of the total energy (blue line) for c) NNP and d) pFFA for one dihedral angle (indicated in red) determines the degree of distortion that will occur when the molecule is deposited in a disordered film. The top panels show the degree of distortion found for the specific dihedral angle found in the matrix. The HOMO energy variance, defined by the sketch in the bottom panel varies significantly from molecule to molecule. Molecules with a large HOMO energy variance (see panel b) have a higher degree of intrinsic disorder and hence a lower mobility.

dihedral angles of NNP and pFFA molecules in the matrix is shown, respectively. In the bottom panels, the variation of the total energy and the HOMO energy of the corresponding molecules as a function of the dihedral angle is shown, as computed in the gas phase. The observed distribution of dihedral angles coincides with the minimum of the total energy profile. However, a signifi cant difference in the variance of HOMO energies is observed when comparing NNP and pFFA for the conformational space of dihedral angles accessed in the computed morphologies. This difference in orbital energy variation leads to drastic differences in the internal disorder contribution σ_i, (0.14 eV vs. 0.10 eV) which strongly influences the mobility (0.4×10^{-4} vs. 5.7×10^{-4} cm^2 $V^{-1}s^{-1}$). To quantify this effect, which directly correlates single molecule properties with macroscopic properties of thin fi lms, we defined ΔE_{int}^{HOMO} as the molecule-specifi c variation of the HOMO energy over the range of dihedral angles close to the total energy minimum (ΔE_{int}^{HOMO} = 0.43 eV vs. 0.37 eV for NNP and pFFA, see Table 1 and Supporting Information). Extending this analysis to all HTL materials (Figure 4b), we find a correlation between ΔE_{int}^{HOMO} and the internal energy disorder parameters computed from the morphologies. This indicates that the variation of the HOMO energy in the energetically permissible range of geometries is the main factor contributing to the variation of the carrier mobility in common HTL materials. This relationship between variation in molecular conformations and the disorder was already suggested in literature but could not be fully quantified for realistic systems.[7f,22] While our observations of this effect do not fully address the differences between experimental and theoretical charge mobility, it is nonetheless a significant step in that direction, as the deviations are contained within one order of magnitude. In addition, the approach can be used as a fast single-molecule based screening and selection technique of the chemical compound space.

4. Conclusion

In summary, we have presented a first-principles-based approach to compute the carrier mobility of small-molecule-based organic materials, which is in good agreement with experiment for a mobility range of over ten orders of magnitude. Central to this approach is the ability to quantitatively characterize the polaron energy disorder[11a] and the reorganization energy in the frozen dihedral approximation. Using an effective medium model[17] for the mobility we were able to decompose the contributions to the hole mobility into molecule-specific factors. The molecular dipole moment is identified as the most important factor influencing the charge mobility. For hole-transport layers from molecules exhibiting a moderate intrinsic dipole, the dominant contribution to the variation of the mobility is the intrinsic disorder, arising from the distortion of the molecules within the amorphous material. This observation permits a computationally inexpensive prescreening of materials for novel HTL materials. Furthermore, the workflow is extendible towards the design of small-molecule organic materials for energy conversion. We note that we have applied a pure hopping approach even to crystalline materials with the aim to establish the upper limit in mobility for both disordered and ordered materials presented in this study. However, with this we do not claim that for the latter the band-transport is inapplicable.[23]

5. Experimental Section

OLED Multiscale Workflow (Figure 1): The first step in the calculation was the pre-optimization of a single molecule by means of density functional theory (DFT).[24] Subsequently, the DFT partial charges were extracted[25] and further used in a molecular mechanics simulation for morphology growth,[26] where morphologies of 300 molecules in size were grown and periodically repeated in all directions. The molecules were parameterized according to the general AMBER force field (GAFF)[27] with AM1-BCC partial charges.[28] Two benchmark studies[29] on a wide range of small organic molecules had proved good performance of the GAFF in the prediction of thermodynamic properties. Periodic boundary conditions were applied in three dimensions. The following steps constitute our morphology generation protocol. First, to get an initial configuration, a cubic box was randomly filled with the molecules. The box size was adjusted to the density 0.9 g cm^{-3}. Then, the energy of the system was minimized to remove unphysical close contacts between atoms. Further, the velocities of the atoms were generated according to the temperature 800 K followed by a short 10 ps NVT (constant number of particles, constant volume, constant temperature) run in order to equilibrate the velocity distribution. NPT (constant number of particles, pressure, temperature) equilibration for 1 ns at 800 K. During this step, we checked (i) that the mean squared displacement of center of mass of molecules was larger than the characteristic length scale of the molecule ensuring that the system was in a liquid state and (ii) that the density of the system was equilibrated to the pressure 1 bar. Then the system was cooled down from 800 to 300 K with the cooling rate 100 K ns^{-1} during NPT run. Last, the final NPT equilibration takes place for 2 ns at 300 K to collect data. During this step we check that the mean squared displacement of center of mass of molecules is virtually zero indicating that the system is in a solid state, where the molecular motion is constrained by the neighbor molecules and only thermal vibrations take place. The Quantum Patch method[11a] was used to extract the electronic structure parameters, e.g., the hopping matrix elements and the on-site polaron energies. For the calculation of reorganization energy we used both Nelsens[14] four point approach as well as the novel frozen dihedral approach, described in the text. Apart from the total disorder variance σ, the variance of intrinsic disorder σ_i was calculated, where distorted molecules from the matrix were used to calculate the disorder of single molecule energy levels. Finally, the parameters are fed into our GEMM approach[17] from which the charge mobility of the thin films are obtained. All quantum mechanical DFT calculations were performed with the quantum chemistry package TURBOMOLE[24] using the RI-approximation. If not indicated different, all DFT calculations were performed with the B3-LYP[30] functional and the def-SV(P) basis set.[31] Reorganization energies were calculated using the B3-LYP[30] functional and a def2-TZVP basis-set.[32]

Materials: The full names of the used materials were tris(8-hydroxyquinolinato)aluminum (Alq_3), N4,N4′-di(biphenyl-3-yl)-N4,N4′-diphenylbiphenyl-4,4′-diamine (mBPD), N1,N4-di(naphthalen-1-yl)-N1,N4-diphenylbenzene-1,4-diamine (NNP), 1,1-bis-(4,4′-diethylaminophenyl)-4,4-diphenyl-1,3,butadinene (DEPB), *N,N′*-bis(1-naphthyl)-*N,N′*-diphenyl-1,1′-biphenyl-4,4′-diamine (α-NPD), *N,N′*-diphenyl-*N,N′*-bis-(3-methylphenylene)-1,10-diphenyl-4,40-diamine (TPD), *N,N′*-bis-[9,9-dimethyl-2-fluorenyl]-*N,N′*-diphenyl-9,9-dimethylfluorene-2,7-diamine (pFFA), tetracene (TET) and pentacene (PEN).

Supporting Information

Supporting Information is available from the Wiley Online Library or from the author.

Acknowledgements

The authors acknowledge funding by the EU project MMM@HPC the STN-DFG project MODEOLED and the Helmholtz program "Science and Technology of Nanosystems" (STN). This work was performed on the computational resource bwUniCluster funded by the Ministry of Science, Research and the Arts Baden-Württemberg and the Universities of the State of Baden-Württemberg, Germany, within the framework program bwHPC and on the computational resource ForHLR Phase I funded by the Ministry of Science, Research and the Arts Baden-Württemberg and DFG ("Deutsche Forschungsgemeinschaft"). Furthermore the authors thank the Carl-Zeiss Foundation for funding the project "Multiskalen Modellierung elektronischer Eigenschaften von Materialien in der organischen Elektronik."

[1] a) C. Groves, *Nat. Mater.* **2013**, *12*, 597; b) L. S. Hung, C. H. Chen, *Mater. Sci. Eng., R* **2002**, *39*, 143; c) T. Kalyani, S. J. Dhoble, *Renewable Sustainable Energy Rev.* **2012**, *16*, 2696; d) M. Mesta, M. Carvelli, R. J. de Vries, H. van Eersel, J. J. M. van der Holst, M. Schober, M. Furno, B. Lüssem, K. Leo, P. Loebl, R. Coehoorn, P. A. Bobbert, *Nat. Mater.* **2013**, *12*, 652; e) *Nat. Mater.* **2015**, *14*, 453.

[2] a) M. A. Green, K. Emery, Y. Hishikawa, W. Warta, E. D. Dunlop, *Prog. Photovoltaics* **2012**, *20*, 12; b) S. Shrestha, *Prog. Photovoltaics* **2013**, *21*, 1429.

[3] N. Karl, *Mol. Cryst. Liq. Cryst.* **1989**, *171*, 31.

[4] R. A. Marcus, *Annu. Rev. Phys. Chem.* **1964**, *15*, 155.

[5] V. Stehr, J. Pfister, R. F. Fink, B. Engels, C. Deibel, *Phys. Rev. B* **2011**, *83*, 155208.

[6] A. Troisi, *Chem. Soc. Rev.* **2011**, *40*, 2347.

[7] a) R. Coehoorn, W. Pasveer, P. Bobbert, M. Michels, *Phys. Rev. B* **2005**, *72*, 155206; b) Y. Roichman, Y. Preezant, N. Tessler, *Phys. Status Solidi A* **2004**, *201*, 1246; c) S. Baranovskii, *Phys. Status Solidi B* **2014**, *251*, 487; d) I. Fishchuk, A. Kadashchuk, S. Hoffmann, S. Athanasopoulos, J. Genoe, H. Bässler, A. Köhler, *Phys. Rev. B* **2013**, *88*, 125202; e) J. Cottaar, L. Koster, R. Coehoorn, P. Bobbert, *Phys. Rev. Lett.* **2011**, *107*, 136601; f) M Van der Auweraer, F. C. De Schryver, P. M. Borsenberger, H. Bässler, *Adv. Mater.* **1994**, *6*, 199; g) H. Bässler, *Phys. Status Solidi B* **1981**, *107*, 9.

[8] a) J. J. Kwiatkowski, J. Nelson, H. Li, J. L. Bredas, W. Wenzel, C. Lennartz, *Phys. Chem. Chem. Phys.* **2008**, *10*, 1852; b) C. Lee, R. Waterland, K. Sohlberg, *J. Chem. Theory Comput.* **2011**, *7*, 2556; c) P. Kordt, J. J. van der Holst, M. Al Helwi, W. Kowalsky, F. May, A. Badinski, C. Lennartz, D. Andrienko, *Adv. Funct. Mater.* **2015**, *25*, 1955; d) B. Baumeier, F. May, C. Lennartz, D. Andrienko, *J. Mater. Chem.* **2012**, *22*, 10971.

[9] S. M. Ryno, C. Risko, J.-L. Brédas, *J. Am. Chem. Soc.* **2014**, *136*, 6421.

[10] H. Bässler, *Phys. Status Solidi B* **1993**, *175*, 15.

[11] a) P. Friederich, F. Symalla, V. Meded, T. Neumann, W. Wenzel, *J. Chem. Theory Comput.* **2014**, *10*, 3720; b) P. Friederich, V. Meded, F. Symalla, M. Elstner, W. Wenzel, *J. Chem. Theory Comput.* **2015**, *11*, 560.

[12] S. Schiefer, M. Huth, A. Dobrinevski, B. Nickel, *J. Am. Chem. Soc.* **2007**, *129*, 10316.

[13] V. Rühle, A. Lukyanov, F. May, M. Schrader, T. Vehoff, J. Kirkpatrick, B. Baumeier, D. Andrienko, *J. Chem. Theory Comput.* **2011**, *7*, 3335.

[14] S. F. Nelsen, S. C. Blackstock, Y. Kim, *J. Am. Chem. Soc.* **1987**, *109*, 677.

[15] H. Li, L. Duan, D. Zhang, Y. Qiu, *J.Phys. Chem. C* **2014**, *118*, 14848.

[16] P. O. Löwdin, *J. Chem. Phys.* **1950**, *18*, 365.

[17] V. Rodin, F. Symalla, P. Friederich, V. Meded, D. Danilov, A. Poschlad, G. Nelles, F. von Wrochem, W. Wenzel, *Phys. Rev. B* **2015**, *91*, 15.

[18] P. Borsenberger, H. Bässler, *J. Chem. Phys.* **1991**, *95*, 5327.

[19] A. Dieckmann, H. Bässler, P. Borsenberger, *J. Chem. Phys.* **1993**, *99*, 8136.

[20] H. Klauk, M. Halik, U. Zschieschang, G. Schmid, W. Radlik, W. Weber, *J. Appl. Phys.* **2002**, *92*, 5259.

[21] S. Engelbrecht, M. Prinz, T. Arend, R. Kersting, *Appl. Phys. Lett.* **2014**, *105*, 012101.

[22] K. M. Weitzel, H. Bässler, *J. Chem. Phys.* **1986**, *84*, 1590.

[23] V. Coropceanu, J. Cornil, D. A. da Silva Filho, Y. Olivier, R. Silbey, J.-L. Brédas, *Chem. Rev.* **2007**, *107*, 926.

[24] R. Ahlrichs, M. Bär, M. Häser, H. Horn, C. Kölmel, *Chem. Phys. Lett.* **1989**, *162*, 165.

[25] U. C. Singh, P. A. Kollman, *J. Comput. Chem.* **1984**, *5*, 129.

[26] H. J. C. Berendsen, D. van derSpoel, R. van Drunen, *Comput. Phys. Commun.* **1995**, *91*, 43.

[27] J. Wang, R. M. Wolf, J. W. Caldwell, P. A. Kollman, D. A. Case, *J. Comput. Chem.* **2004**, *25*, 1157.

[28] a) A. Jakalian, B. L. Bush, D. B. Jack, C. I. Bayly, *J. Comput. Chem.* **2000**, *21*, 132; b) A. Jakalian, D. B. Jack, C. I. Bayly, *J. Comput. Chem.* **2002**, *23*, 1623.

[29] a) C. Caleman, P. J. van Maaren, M. Hong, J. S. Hub, L. T. Costa, D. van der Spoel, *J. Chem. Theory Comput.* **2012**, *8*, 61; b) J. Wang, T. Hou, *J. Chem. Theory Comput.* **2011**, *7*, 2151.

[30] A. D. Becke, *J. Chem. Phys.* **1993**, *98*, 1372.

[31] A. Schafer, H. Horn, R. Ahlrichs, *J. Chem. Phys.* **1992**, *97*, 2571.

[32] A. Schafer, C. Huber, R. Ahlrichs, *J. Chem. Phys.* **1994**, *100*, 5829.

[33] a) H. H. Fong, S. K. So, *J. Appl. Phys.* **2006**, *100*, 094502; b) S. Naka, H. Okada, H. Onnagawa, Y. Yamaguchi, T. Tsutsui, *Synth. Met.* **2000**, *111*, 331; c) R. Kepler, P. Beeson, S. Jacobs, R. Anderson, M. Sinclair, V. Valencia, P. Cahill, *Appl. Phys. Lett.* **1995**, *66*, 3618; d) J. Kalinowski, N. Camaioni, P. Di Marco, V. Fattori, A. Martelli, *Appl. Phys. Lett.* **1998**, *72*, 513; e) A. G. Mückl, S. Berleb, W. Brütting, M. Schwoerer, *Synth. Met.* **2000**, *111*, 91.

[34] K. Okumoto, K. Wayaku, T. Noda, H. Kageyama, Y. Shirota, *Synth. Met.* **2000**, *111*, 473.

[35] P. Borsenberger, J. Shi, *Phys. Status Solidi B* **1995**, *191*, 461.

[36] T. Mori, E. Sugimura, T. Mizutani, *J. Phys. D: Appl. Phys.* **1993**, *26*, 452.

[37] S. Tse, K. Kwok, S. So, *Appl. Phys. Lett.* **2006**, *89*, 262102.

[38] M. Stolka, J. Yanus, D. Pai, *J. Phys. Chem.* **1984**, *88*, 4707.

[39] R. De Boer, T. Klapwijk, A. Morpurgo, *Appl. Phys. Lett.* **2003**, *83*, 4345.